



## Triazolo[4,5-*d*]pyrimidin-5-amines based ERK3 inhibitors fail to demonstrate selective effects on adipocyte function

Andrei Belykh<sup>a</sup>, Izabela Hawro<sup>a</sup>, Katarzyna Kolczyńska-Matysiak<sup>a</sup>, Angel Loza-Valdes<sup>a</sup>, Adam Mieczkowski<sup>b</sup>, Grzegorz Sumara<sup>a,\*</sup>

<sup>a</sup> Nencki Institute of Experimental Biology, Polish Academy of Sciences, 3 Pasteur Street, 02-093 Warsaw, Poland

<sup>b</sup> Institute of Biochemistry and Biophysics, Polish Academy of Sciences, 5a Pawlowskiego, 02-106 Warsaw, Poland

### ARTICLE INFO

#### Keywords:

ERK3  
MAPK6  
Adipocytes  
Metabolism  
Triazolo[4,5-*d*]pyrimidin-5-amines  
Inhibitors

### ABSTRACT

Extracellular signal-regulated kinase 3 (ERK3 also designated MAPK6 — mitogen-activated protein kinase 6) is a ubiquitously expressed kinase participating in the regulation of a broad spectrum of physiological and pathological processes. Targeted inhibition of the kinase may allow the development of novel treatment strategies for a variety of types of cancer and somatic pathologies, as well as preserving metabolic health, combat obesity and diabetes. We chose and synthesized three triazolo [4,5-*d*]pyrimidin-5-amines proposed previously as putative ERK3 inhibitors to assess their selectivity and biological effects in terms of metabolic state impact in living cells. As it was previously shown that ERK3 is a major regulator of lipolysis in adipocytes, we focused on this process. Our new results indicate that in addition to the previously identified lipolytic enzyme ATGL, ERK3 also regulates hormone-sensitive lipase (HSL) and monoglyceride lipase (MGL). Moreover, this kinase also promotes the abundance of fatty acid synthase (FASN) as well as protein kinase cAMP-activated catalytic subunit alpha (PKAC $\alpha$ ). To investigate various effects of putative ERK3 inhibitors on lipolysis, we utilized different adipocyte models. We demonstrated that molecules exhibit lipolysis-modulating effects; however, the effects of triazolo [4,5-*d*]pyrimidin-5-amines based inhibitors on lipolysis are not dependent on ERK3. Subsequently, we revealed a wide range of the compounds' possible targets using a machine learning-based prediction.

Therefore, the tested compounds inhibit ERK3 *in vitro*, but the biological effect of this inhibition is significantly overlapped and modified by some other molecular events related to the non-selective binding to other targets.

### 1. Introduction

Extracellular signal-regulated kinase 3 (ERK3) is a ubiquitously expressed serine-threonine kinase that belongs to the “atypical” subfamily of mitogen-activated protein kinases (hence also designated MAPK6 — mitogen-activated protein kinase 6) [1–3]. ERK3 signaling plays a role in various physiological and pathological conditions. The biological functions of ERK3 include, but are not limited to, the regulation of cell proliferation, migration and invasion, cell-cycle progression, cellular differentiation, cytoskeletal dynamics, and transcriptional control [4–8]. The role of ERK3 in regulating cell cycle progression becomes particularly evident during carcinogenesis. Several recent studies have demonstrated that ERK3 overexpression significantly promotes the growth of various human cancer cell lines, such as prostate cancer PC3 and DU145, ovarian cancer OVCA433, breast cancer SUM159, and non-small cell lung cancer H1299 cells [9]. Consistently,

ERK3 knocking down suppresses the proliferation, migration, and invasion potential of different cancer cells, including cervical cancer [10], breast cancer [11,12], and human lung carcinomas [13,14].

However, the clinical importance of ERK3 goes far beyond oncology. It is also involved in the mechanisms of podocyte injury during diabetic nephropathy [15], as well as renal fibrosis [16]. Up-regulation of ERK3 weakens the development of protective mechanisms against myocardial ischemia-reperfusion injury [17]. Furthermore, ERK3 expression is elevated in human visceral adipose tissue isolated from obese patients [18]. An earlier study defined the crucial role of ERK3 in the regulation of adipose tissue function. ERK3 was identified as a major signaling node activating hormonally evoked degradation of triglycerides (lipolysis) in adipose tissue. Moreover, the deletion of this kinase, specifically in adipocytes, elevates energy expenditure, which counters obesity and associated diabetes [18,19]. All of this makes ERK3 a promising therapeutic target for the treatment of a wide range of diseases.

\* Corresponding author.

E-mail address: [g.sumara@nencki.edu.pl](mailto:g.sumara@nencki.edu.pl) (G. Sumara).

<https://doi.org/10.1016/j.abbi.2023.109825>

Received 25 July 2023; Received in revised form 24 October 2023; Accepted 17 November 2023

Available online 20 November 2023

0003-9861/© 2023 The Authors. Published by Elsevier Inc. This is an open access article under the CC BY license (<http://creativecommons.org/licenses/by/4.0/>).

Nevertheless, there are no specific and selective ERK3 inhibitors reported so far that have been validated in the biological systems. Currently, only weak ERK3 inhibitors have been identified, including the multi-kinase inhibitor Crizotinib [2,5,20,21]. In 2020, Grädler et al. described the identification and profiling of potent and selective triazolo [4,5-*d*]pyrimidin-5-amines based ERK3 inhibitors [2]. They demonstrated high binding properties and biochemical potency of the studied compounds using a broad spectrum of binding assays (kinase selectivity screen, microscale thermophoresis (MST), enzyme-coupled ADP-Glo, NanoBret) and by applying both full-length and recombinant ERK3 proteins in different phosphorylation state together with the kinase substrate MK5 (MAP kinase-activated protein kinase 5 also designated PRAK — p38-regulated and -activated kinase). However, there is no information available regarding the selectivity of their action, as well as the biological effects of the compounds in living cells.

Given that ERK3 inhibition could preserve metabolic health and combat obesity and diabetes [18,19], we decided, for the first time, to examine certain chemicals proposed by Grädler et al. [2] and evaluate their biological properties and specificity in adipocytes which defines the novelty of this study. We selected the three most promising compounds. *Compound 7* (C7, Fig. S1A) was previously described by Dorsch et al. [22]. It demonstrated a high binding affinity and potency (MST binding in the dissociation constant ( $K_d$ ) range of 0.16–0.89  $\mu$ M and a half-maximal inhibitory concentration ( $IC_{50}$ ) in the range of 0.3–0.549  $\mu$ M, depending on the assay used and the tested ERK3 fragment). It also promoted an active kinase conformation, ruling out the phosphorylation of ERK3 Ser<sup>189</sup>, as indicated by crystallography data [2]. It's worth noting that ERK3, phosphorylated in the activation loop motif SEG at Ser<sup>189</sup>, even in unstimulated cells [1], is both essential and sufficient for its ability to interact with, phosphorylate, and activate its best-characterized downstream substrate, MK5, both *in vitro* and *in vivo* [23]. Other substances (including those studied in the current research) were chosen from the author's corporate compound library based on the ERK3•C7 crystal structure. *Compound 18* (C18, Fig. S1B) was among the most potent compounds (NanoBRET  $IC_{50}$  = 38 nM, biochemical  $IC_{50}$  73–93 nM). It has identical crystallography binding modes compared to C7 (binding in the ATP site with the A-loop, GC-loop, and  $\alpha$ C-helix conformations and potential conformational impact on MK5 recognition) and displayed an attractive selectivity profile, with only 2 out of 389 kinases inhibited above 80 % at 1  $\mu$ M. *Compound 20* (C20, Fig. S1C) exhibited the best potency (NanoBRET  $IC_{50}$  = 13 nM, biochemical  $IC_{50}$  30–55 nM) among the other described compounds [2].

In our study, we employed various adipocyte models and demonstrated that two molecules (C7 and C20) unexpectedly exhibit a persistent pro-lipolytic effect, while C18's action is ambivalent: anti-lipolytic in  $\beta$ -adrenergic-induced conditions and pro-lipolytic without stimulation. These effects are largely ERK3-independent; however, the decrease in ERK3 and MK5 protein levels with treatment and a few events suggest at least partial involvement of ERK3 in the mechanism of the compounds' action. We suggest that the tested compounds can inhibit ERK3 *in vitro*, but the biological effect of this inhibition is significantly overlapped and modified by some other molecular events related to their non-selective binding to other targets. Subsequently, we uncovered a wide range of possible targets for the compounds using a machine learning-based prediction. Another important result of this study was the first discovered diminution of PKAC $\alpha$ , as well as some lipolytic and lipogenic enzymes observed upon ERK3 silencing.

## 2. Materials and methods

### 2.1. Compounds synthesis and usage

The inhibitors used in this study were synthesized according to literature procedures [22]. Additional information about the different spectral analyses of the compounds can be found in Figs. S2–S30.

**Synthesis of C7** — (1*R*,4*R*)-*N*<sup>1</sup>-(3-(4-methoxyphenyl)-3*H*- [1-3]

triazolo [4,5-*d*]pyrimidin-5-yl)cyclohexane-1,4-diamine (Fig. S1D): (1*R*,4*R*)-cyclohexane-1,4-diamine (1) (1.33 g, 11.63 mmol, 2.03 equiv.) and 5-chloro-3-(4-methoxyphenyl)-3*H*- [1-3]triazolo [4,5-*d*]pyrimidine (2) (1.50 g, 5.73 mmol, 1.00 equiv) were heated in 20 ml of methoxyethanol in 80 °C for 3 h. Then, volatiles were evaporated under the reduced pressure and the residue was re-dissolved in methanol followed by evaporation with silica gel. Chromatography: 10–20 % methanol in chloroform followed by TEA:MeOH:CHCl<sub>3</sub> 1:20:80. Yield: 1.1 g (57 %). Mp.: 195.5–196.6 °C. In NMR spectra this compound exists in two main forms, in approx. 2:1 ratio.

<sup>1</sup>H NMR (500 MHz, DMSO-*d*<sub>6</sub>)  $\delta$  9.32, 9.24 (2  $\times$  s, 1H, H<sub>Ar</sub> pyrimidine); 8.15–7.89 (m, 3H, 2  $\times$  H<sub>Ar</sub> *p*-anisidine overlapped with NH signal); 7.89–7.42 (wave, 2H, NH<sub>2</sub>); 7.21–7.11 (m, 2H, H<sub>Ar</sub> *p*-anisidine); 3.85 (s, 3H, CH<sub>3</sub>); 3.77–3.61 (m, 1H, CH); 3.05–2.90 (m, 1H, CH); 2.14–1.90 (m, 4H, 2  $\times$  CH<sub>2</sub>); 1.51–1.28 (m, 4H, 2  $\times$  CH<sub>2</sub>); <sup>13</sup>C NMR (100 MHz, DMSO-*d*<sub>6</sub>)  $\delta$  160.8 (C<sub>Ar</sub><sup>IV</sup>); 158.9, 158.7 (C<sub>Ar</sub><sup>IV</sup>); 153.4, 153.3 (CH<sub>Ar</sub> pyrimidine); 150.4, 149.7 (C<sub>Ar</sub><sup>IV</sup>); 131.0, 130.7 (C<sub>Ar</sub><sup>IV</sup>); 128.9, 128.6 (C<sub>Ar</sub><sup>IV</sup>); 123.3, 122.4 (CH<sub>Ar</sub> *p*-anisidine); 114.6 (CH<sub>Ar</sub> *p*-anisidine); 55.6 (CH<sub>3</sub>); 49.4, 49.2, 48.8 (CH); 30.1, 29.34, 29.31 (CH<sub>2</sub>); HRMS (ESI): *m/z* [M+H]<sup>+</sup> calcd for C<sub>17</sub>H<sub>22</sub>N<sub>7</sub>O: 340.18803, found: 340.18811;

**Synthesis of C18** — (R)-3-(4-methoxyphenyl)-*N*-(1-(pyridin-4-yl)pyrrolidin-3-yl)-3*H*- [1-3]triazolo [4,5-*d*]pyrimidin-5-amine (Fig. S1E): (R)-1-(pyridin-4-yl)pyrrolidin-3-amine (3) (100 mg, 0.61 mmol, 1 equiv.) and 5-chloro-3-(4-methoxyphenyl)-3*H*- [1-3]triazolo [4,5-*d*]pyrimidine (2) (160 mg, 0.61 mmol, 1 equiv.) were dissolved in 5 mL of methoxyethanol followed by addition of triethylamine (86  $\mu$ L, 0.61 mmol, 1 equiv.). The reaction mixture was heated in 80 °C for 3 h, then volatiles were evaporated under the reduced pressure and the residue was re-dissolved in methanol followed by evaporation with silica gel. Chromatography: 10–20 % methanol in chloroform. Yield: 112 mg (47 %). Mp.: 210 °C (decomposition).

In NMR spectra this compound exists in two forms, in approx. 7:3 ratio (based on CH pyrimidine, CH pyrrolidine and NH signals). <sup>1</sup>H NMR (500 MHz, DMSO-*d*<sub>6</sub>)  $\delta$  9.38, 9.28 (2  $\times$  s, 1H, CH<sub>Ar</sub> pyrimidine); 8.56–8.44, 8.34–8.33 (2  $\times$  m, 1H, NH); 8.13–7.86 (m, 4H, 2  $\times$  CH<sub>Ar</sub> pyridine + 2  $\times$  CH<sub>Ar</sub> *p*-anisidine); 7.17 (d, 2H, *J* = 8.5 Hz, CH<sub>Ar</sub> *p*-anisidine); 6.49–6.46 (m, 2H, CH<sub>Ar</sub> pyridine); 4.80–4.67, 4.65–4.52 (m, 1H, CH); 3.84 (s, 1H, Me); 3.75–3.59 (m, 1H, CH<sub>2</sub>); 3.55–3.46 (m, 1H, CH<sub>2</sub>); ~3.34 (m, 2H, 1  $\times$  CH<sub>2</sub> + 1  $\times$  CH<sub>2</sub><sup>o</sup>, overlapped with H<sub>2</sub>O signal); 2.40–2.24 (m, 1H, CH<sub>2</sub><sup>o</sup>); 2.23–2.04 (m, 1H, CH<sub>2</sub><sup>o</sup>); <sup>13</sup>C NMR (100 MHz, DMSO-*d*<sub>6</sub>)  $\delta$  161.1 (C<sub>Ar</sub><sup>IV</sup>); 158.9, 158.8 (C<sub>Ar</sub><sup>IV</sup>); 153.5, 153.3 (CH<sub>Ar</sub> pyrimidine); 151.3 (C<sub>Ar</sub><sup>IV</sup>); 149.6, 149.3 (CH<sub>Ar</sub> pyridine); 131.3, 131.0 (C<sub>Ar</sub><sup>IV</sup>); 128.9, 128.6 (C<sub>Ar</sub><sup>IV</sup>); 123.5, 122.6 (CH<sub>Ar</sub> *p*-anisidine); 114.8, 114.7 (CH<sub>Ar</sub> *p*-anisidine); 107.0 (CH<sub>Ar</sub> pyridine); 55.5 (OMe); 52.4, 51.9 (CH<sub>2</sub>); 51.3, 50.9 (CH); 45.2 (CH<sub>2</sub>); 30.5, 30.0 (CH<sub>2</sub>); HRMS (ESI): *m/z* [M+H]<sup>+</sup> calcd for C<sub>20</sub>H<sub>21</sub>N<sub>8</sub>O: 389.18328, found: 389.18325.

**Synthesis of C20** — 3-(4-ethoxyphenyl)-*N*-(1-(1-methylpiperidin-4-yl)-1*H*-pyrazol-4-yl)-3*H*- [1-3]triazolo [4,5-*d*]pyrimidin-5-amine (Fig. S1F): 1-(1-methylpiperidin-4-yl)-1*H*-pyrazol-4-amine (4) (765 mg, 2.77 mmol, 1 equiv.) and 5-chloro-3-(4-ethoxyphenyl)-3*H*- [1-3]triazolo [4,5-*d*]pyrimidine (5) (500 mg, 2.77 mmol, 1 equiv.) were dissolved in 10 mL of methoxyethanol followed by addition of triethylamine (0.39 mL, 2.77 mmol, 1 equiv.). The reaction mixture was heated in 80 °C for 3 h, then volatiles were evaporated under the reduced pressure and the residue was re-dissolved in methanol followed by evaporation with silica gel. Chromatography: 10–20 % methanol in chloroform. Yield: 960 mg (82 %). Mp.: 234 °C (decomposition).

In NMR spectra this compound exists in two forms, in approx. 17:3 ratio (based on NH signal). <sup>1</sup>H NMR (500 MHz, DMSO-*d*<sub>6</sub>)  $\delta$  10.41, 10.09 (2  $\times$  s, 1H, NH); 9.34 (s, 1H, CH<sub>Ar</sub> pyrimidine); 8.05 (s, 1H, CH<sub>Ar</sub> pirazole); 7.97 (d, 2H, *J* = 8.5 Hz, CH<sub>Ar</sub> *p*-phenetidine); 7.67 (s, 1H, CH<sub>Ar</sub> pirazole); 7.23 (d, 2H, *J* = 8.5 Hz, CH<sub>Ar</sub> *p*-phenetidine); 4.43–4.24 (m, 1H, CH); 4.14 (q, 2H, *J* = 7.0 Hz, CH<sub>2</sub> Et); 3.31–3.22 (m, 2H, CH<sub>2</sub> piperazine, overlapped with H<sub>2</sub>O signal); 2.97–2.76 (m, 2H, CH<sub>2</sub> piperazine); 2.60 (s, 3H, Me-N); 2.28–2.03 (m, 4H, 2  $\times$  CH<sub>2</sub> piperazine); 1.38 (t, 3H, *J* = 7.0 Hz, Me Et); <sup>13</sup>C NMR (100 MHz, DMSO-*d*<sub>6</sub>)  $\delta$  158.3 (C<sub>Ar</sub><sup>IV</sup>); 158.1 (C<sub>Ar</sub><sup>IV</sup>); 153.4 (CH<sub>Ar</sub>

pyrimidine); 149.6 ( $C_{Ar}^{IV}$ ); 130.1 ( $CH_{Ar}$  pirazole); 130.1 ( $C_{Ar}^{IV}$ ); 128.4 ( $C_{Ar}^{IV}$ ); 122.9 ( $CH_{Ar}$  p-phenetidine); 122.2 ( $C_{Ar}^{IV}$ ); 117.9 ( $CH_{Ar}$  pirazole); 115.3 ( $CH_{Ar}$  p-phenetidine); 63.6 ( $CH_{2Et}$ ); 55.8 (CH); 52.5 ( $CH_2$  piperidine); 43.3 (Me-N); 29.8 ( $CH_2$  piperidine); 14.7 (Me<sub>Et</sub>); HRMS (ESI):  $m/z$  [M+H]<sup>+</sup> calcd for C<sub>21</sub>H<sub>26</sub>N<sub>9</sub>O: 420.22548, found: 420.22549.

Reactions were monitored by thin-layer chromatography (TLC), using silica gel plates (Kieselgel 60F<sub>254</sub>, E. Merck, Darmstadt, Germany). Column chromatography was performed using silica gel 60 M (0.040–0.063 mm, E. Merck, Darmstadt, Germany). Melting points are uncorrected and were measured using a Büchi (New Castle, DE, USA) Melting Point B-540 apparatus. The <sup>1</sup>H NMR and <sup>13</sup>C NMR spectra were recorded in DMSO-*d*<sub>6</sub> and CD<sub>3</sub>OD at the Department of Chemistry, University of Warsaw, using an AVANCE III HD 500 MHz spectrometer (Bruker, Billerica, MA, USA); shift values in parts per million are relative to the SiMe<sub>4</sub> internal reference. Multiplets were assigned as s (singlet), d (doublet), t (triplet) q (quartet), and m (multiplet). High-resolution mass spectra were recorded using the LTQ Orbitrap Velos instrument (Thermo Scientific, Waltham, MA, USA) at the Laboratory of Mass Spectrometry, Institute of Biochemistry and Biophysics, PAS (Warsaw, Poland).

Compounds were dissolved in dimethyl sulfoxide (DMSO, Sigma-Aldrich, cat. #D8418) at a 15–20 mM stock concentration, aliquoted by 10 µl, and stored at –80 °C. Final concentrations of the tested molecules were prepared *ex tempore* by dissolving stock solutions in the medium. Control (0 µM) groups received volumes of DMSO equivalent to the groups treated with compounds in the highest concentration.

## 2.2. Cell culture

3T3-L1 preadipocyte cells were cultured and maintained in culture medium (M1) containing high glucose Dulbecco's modified Eagle's medium (DMEM High Glucose, Biowest, cat #L0101), supplemented with 10 % fetal bovine serum (FBS, Gibco, cat # 10270106), 4 mM glutamine (GlutaMAX, Gibco, cat # 35050061), 1 mM sodium pyruvate (Gibco, cat # 11360070), and 1 % Penicillin-Streptomycin (Gibco, cat # 15140122). The medium was changed every 2 days until the cells reached confluence. Two days after reaching confluence, 3T3-L1 cell differentiation into adipocytes was induced according to the standard procedure described by Löfler et al. (2018) [24]. Briefly, culture medium (M2), supplemented with 2 µM dexamethasone (Sigma-Aldrich, cat #D2915), 0.5 mM 3-Isobutyl-1-methylxanthine (IBMX, Sigma-Aldrich, cat #I5879), and 1.5 µg/ml insulin (Sigma-Aldrich, I9278), was added to the cells on Day 0 and Day 2. On Days 4, 6, 8, and 10, culture medium (M3) with only 1.5 µg/ml insulin was used to maintain the cells, and experiments were initiated on Day 12.

Stromal vascular cells (SVCs) were isolated from subcutaneous white adipose tissue (subWAT) of 5- to 9-week-old mice, as previously described by Löfler et al. (2018) [24]. In brief, subWAT from mice was isolated, cleaned (lymph nodes were removed), minced, and digested in Dulbecco's Phosphate Buffered Saline (DPBS, Biowest, cat #L0615) containing 1 mg/mL Collagenase P (Roche, cat # 11249002001), 5 mM CaCl<sub>2</sub>, 1 % bovine serum albumin (BSA, BioShop, cat # ALB001.500), and 1 % Penicillin-Streptomycin for 30 min at 37 °C with constant agitation at 400 rpm. Adipose tissue was then passed through a 40-µm mesh, washed once in DPBS, and twice in medium by centrifugation, and plated on Matrigel-coated (Corning) plates in culture medium (M1): DMEM/F-12 (Biowest, cat #L0090) containing 10 % FBS, 1 % MEM Non-Essential Amino Acids (NEAA, Gibco, cat. # 11140035), 0.1 mM β-mercaptoethanol (Gibco, cat # 21985023), 1 mM sodium pyruvate, and 20 µg/mL gentamicin (Gibco, cat # 15750060). The culture medium was changed every 2 days until the cells reached confluence. Preadipocyte differentiation was induced by 0.2 µM indomethacin (Sigma-Aldrich, cat #I7378), 2 µM dexamethasone, 0.5 mM IBMX, 0.5 µM rosiglitazone (Sigma-Aldrich, cat #R2408), and 1.5 µg/ml insulin on Day 0 (two days after confluence) and Day 2. On Days 4 and 6, medium with only 1.5 µg/ml insulin was used to maintain cells, and experiments

were initiated on Day 9.

Stable cell lines with long-term gene silencing of the *Erk3* gene (shERK3), as well as non-targeting control cells (shNTC), were obtained from previous experiments. Detailed information on the generation of these lines can be found in El-Merahbi et al. (2020) [19].

## 2.3. Cytotoxicity assays

Two days prior to viability assays experiments (on differentiation Days 10 and 7 for 3T3-L1 and SVC, respectively), adipocytes were replated from a Petri dish to a 96-well cell culture plate. Cells were washed with DPBS and subjected to Accutase (Sigma-Aldrich, cat. # A6964) for detachment activation. The adipocyte suspension from Petri dishes was then transferred to 15 ml conical tubes and centrifuged at room temperature for 5 min at 1250 rpm. The medium supernatant was aspirated, and the cellular pellet was resuspended in culture medium (M1). After counting the adipocytes, they were seeded onto 96-well cell culture plates pre-coated with 0.5 % Matrigel (Matrigel Basement Membrane Matrix, Corning, cat. # 356234) at a density of 5.5 × 10<sup>4</sup> cells per well in 200 µl of culture medium (M1) and left for 48 h. Then, the adipocytes were treated with the investigated compounds for 24 h, and tests were performed right after this according to the manufacturer's instructions.

During the MTT test (CyQUANT MTT Cell Viability Assay, Invitrogen, cat. #V13154), cells were washed with DPBS, and a mixture (1:10 v/v) of MTT stock solution and phenol red-free DMEM (Gibco, cat # A1443001), supplemented with glucose, glutamine, sodium pyruvate, and penicillin-streptomycin, was added in the volume of 110 µl per well. Cells were incubated for 3.5 h at +37 °C in a CO<sub>2</sub> incubator. 85 µl of MTT/medium mix was aspirated and the remaining 25 µl were diluted in 100 µl DMSO, incubated for 10 min at +37 °C. The plate was gently shaken to dissolve the formazan formed during the test, and the absorbance was read at 540 nm using an Infinite M1000 PRO multimode reader (Tecan, Switzerland). Data were calculated as a percentage ratio of an individual observation to the median value of the control group (0 µM) after subtracting the background absorbance.

To perform the CTB test (CellTiter-Blue Cell Viability Assay, Promega, cat. #G8080), cells were washed with DPBS and then incubated with the 10 % CTB solution (100 µl/well) in culture medium (M1) for 90 min at +37 °C in a CO<sub>2</sub> incubator. The absorbance was measured using an Infinite M1000 PRO multimode reader (Tecan, Switzerland), and the difference between the measurement (570 nm) and the reference measurement (600 nm) was used for further calculations (negative values were equalized to zero). Data were calculated as a percentage ratio of an individual observation to the median value of the control group (0 µM) after subtracting the background absorbance.

The procedure of the crystal violet test included the following steps. First, adipocytes were washed twice with DPBS, and 100 µl/well of 70 % ethanol was added to fix the cells for 30 min. After removing the ethanol, the plate was air-dried overnight. Then, 100 µl/well of a 0.5 % crystal violet (Sigma-Aldrich, cat. #C0775) aqueous solution was used with gentle shaking for 30 min. Crystal violet was aspirated, and the plate was washed with water to remove the excess dye, followed by subsequent overnight air-drying. The next day, 100 µl/well of 10 % acetic acid (Sigma-Aldrich, cat. # A6283) was added for 15 min on a shaker to dissolve the dye. 50 µl of solution from each well was transferred to a new plate and diluted with 150 µl of Milli-Q water. The absorbance was measured using an Infinite M1000 PRO multimode reader (Tecan, Switzerland) at 560 nm. Data were calculated as a percentage ratio of an individual observation to the median value of the control group (0 µM) after subtracting the background absorbance.

## 2.4. Lipolysis assay

Free fatty acids (FFAs) were determined as described by El-Merahbi et al. [19]. Adipocytes were washed twice with DPBS. Then, a culture

medium containing compounds in different concentrations was added to the cells for 20 h. Next, adipocytes were washed twice with DPBS and serum-starved for 2 h in phenol red-free, glucose-free DMEM (Gibco, cat # A1443001), supplemented with 1 % fatty acid-free BSA (Sigma-Aldrich, cat # A8806) and the corresponding dose of compounds. Afterward, the serum-starved medium was replaced either with the same medium containing investigated compounds or with serum-starved medium supplemented by the compounds and 1  $\mu$ M isoproterenol hydrochloride (United States Pharmacopeia, cat # 1351005) for  $\beta$ -adrenergic stimulation for 2 h. The conditioned medium was then collected and analyzed. Release of FFAs in the medium was measured using NEFA reagents (NEFA-HR (2) R1 Set, cat # 434-91795, Fujifilm Wako Chemicals Europe and NEFA-HR (2) R2 Set, cat # 436-91995, Fujifilm Wako Chemicals Europe) according to the manufacturer's instructions. The difference between the absorbance measurement (546 nm) and the reference measurement (660 nm) was used for further calculations. Values were normalized to the cells' total DNA content by Hoechst 33342 staining (Thermo Scientific, cat # 62249; excitation/emission wavelength = 330/470 nm). Values obtained from shERK3 3T3-L1 cells were additionally normalized to those from shNTC 3T3-L1 cells by assessing the cells' intracellular lipid content via the AdipoRed Assay Reagent (Lonza, cat # PT-7009; excitation/emission wavelength = 485/575 nm) for correction of potential differentiation diversity between the lines. All measurements were performed using an Infinite M1000 PRO multimode reader (Tecan, Switzerland).

### 2.5. Western blotting

24 h prior to protein collection, 3T3-L1 adipocytes were started to be treated with investigated compounds, consequently dissolved in the following: culture medium (20 h), starvation medium (2 h), and starvation medium supplemented by 1  $\mu$ M isoproterenol hydrochloride (2 h) to mimic the conditions of the lipolysis assay described above. To extract total proteins, cells were washed thrice with ice-cold DPBS and lysed in cold RIPA Lysis and Extraction Buffer (Thermo Scientific, cat # 89901) supplemented with Halt Protease and Phosphatase Inhibitor Cocktail (Thermo Scientific, cat # 78445), followed by a 10-min centrifugation at 12,000 rpm at +4 °C. The supernatant was collected and stored at -80 °C. Total protein concentration was quantified using a Pierce BCA Protein Assay Kit (Thermo Scientific, cat # 23225). Samples were accordingly diluted to have the same protein concentration, mixed in a 1:1 v/v ratio with a 2  $\times$  Laemmli Sample Buffer supplemented with 3.5 %  $\beta$ -mercaptoethanol, and boiled at +95 °C for 5 min at 300 rpm. Prepared protein extracts were separated on 10 % SDS-PAGE gels by electrophoresis and transferred to PVDF membranes with wet transfer cells. Membranes were blocked in 5 % (w/v) BSA in TBST before overnight probing with the indicated primary antibodies at 4 °C, followed by TBST washes and incubation with the corresponding secondary antibody dissolved in 5 % (w/v) BSA in TBST. The signals were detected on autoradiography film with an enhanced chemiluminescence solution. Antibodies used included recombinant monoclonal rabbit anti-MAPK6/ERK3 (clone EP1720Y; Abcam, cat # ab53277), recombinant monoclonal rabbit anti-MAPKAPK-5 (clone D70A10; Cell Signaling Technology, cat # 7419), polyclonal rabbit anti-ATGL (Cell Signaling Technology, cat # 2138), recombinant monoclonal rabbit anti-HSL (clone D6W5S; Cell Signaling Technology 4107), polyclonal goat anti-MGL (Abcam, cat # ab77398), recombinant monoclonal rabbit anti-FASN (clone C20G5; Cell Signaling Technology, cat #3180), polyclonal rabbit anti-PKAC- $\alpha$  (Cell Signaling Technology, cat #4782), recombinant monoclonal rabbit anti-vinculin (clone E1E9V; Cell Signaling Technology 13901).

### 2.6. Statistical analysis

All statistical analyses and illustrative materials were created using GraphPad Prism v9.5.1 (GraphPad Software, USA). Due to the

predominantly non-normal data distribution, as assessed by the Shapiro-Wilk test, nonparametric methods were employed. To compare more than 2 groups at once, the Kruskal-Wallis test was followed by the uncorrected Dunn's test, with a two-stage linear step-up procedure of Benjamini, Krieger, and Yekutieli for multiple comparisons to control the False Discovery Rate (desired FDR is 0.05). The Mann-Whitney rank-sum test was used for pairwise comparisons, with a two-stage linear step-up procedure of Benjamini, Krieger, and Yekutieli for multiple comparisons to control the FDR (desired FDR (Q) was set at 1 %). Graphs present data as Median and Interquartile range.

IC<sub>50</sub> values (the concentration that inhibited cell viability to 50 % of the control) were calculated using a normalized variable slope model of nonlinear regression analysis with the least squares regression fitting method. This model does not assume a standard slope but rather fits the Hill Slope from the data. The model is represented by the equation:  $Y = 100 / (1 + (IC_{50}/X)^{HillSlope})$ , where X = inhibitor's concentrations, Y = viability (%) normalized to the 0  $\mu$ M group, and HillSlope = unitless slope factor or Hill slope.

## 3. Results

### 3.1. C7 and C20 exhibit unexpected pro-lipolytic effects, while C18's action is ambivalent in 3T3-L1 adipocytes

Since ERK3 drives fatty acids output from adipocytes [18,19], we hypothesized that ERK3 inhibitors would decrease the lipolysis rate. To test this, we decided to examine the metabolic effects of selected compounds in the model of differentiated adipocyte-like 3T3-L1 cells. Prior to testing ERK3 inhibitors for their ability to alter the lipolysis rate, we screened for the cytotoxic effects of the chosen substances to identify a range of doses that did not affect the viability of the cells (Fig. 1 A, C, E, Fig. S31).

Due to possible technical shortcomings, using a single viability assay is associated with the risk of erroneous interpretation [25]. Therefore, it is advisable to test various biological assays to monitor drug-induced cell responses [26]. We chose three simple and sensitive high-throughput analyses — MTT (3-(4,5-dimethylthiazol-2-yl)-2,5-diphenyltetrazolium bromide or tetrazolium), CTB (CellTiter-Blue, also known as Alamar Blue), and crystal violet (crystal violet staining or CVS) — each having different mechanisms of action and allowing us to assess the impact of the test molecules on cell viability, survival, metabolism, and proliferation [25–29].

As it was expected, the results of the viability assessment depend on the test used. While both enzymatic assays showed very consistent values, the non-enzymatic crystal violet staining presented a slight overestimation of viability compared to CTB and MTT in all repetitions. This is in agreement with the fact that it can also count dead attached cells and underestimate cytotoxicity [25].

However, all investigated compounds generally have similar cytotoxic effects on the 3T3-L1 adipocytes, with a significant drop in viability observed after exceeding a concentration of approximately 30  $\mu$ M. The average half maximal inhibitory concentration (IC<sub>50</sub>) in metabolism-dependent assays (Fig. 1, Fig. S31) for all studied molecules was approximately 49  $\mu$ M, with toxicity increasing in the order of C20 < C18 < C7 (average CTB/MTT IC<sub>50</sub> = 45.74  $\mu$ M, 40.72  $\mu$ M, and 39.26  $\mu$ M, respectively).

Despite the cytotoxicity underestimation by the crystal violet assay compared to other assays, it nevertheless reflected the general trend (Fig. S31 A, C, E). Moreover, it revealed an intriguing observation, showing a significant increase in viability (above control values) for low doses of C18. Since CVS correlates with DNA content [25], this increase could be related to a treatment-induced activation of cell proliferation. Considering that ERK3 is a negative regulator of cell proliferation and its inhibition promotes cell growth [5,7,8,30], we view this finding as indirect evidence of the ERK3-dependent mechanism of C18's action.

Based on the cytotoxicity data, we selected a wide range of doses

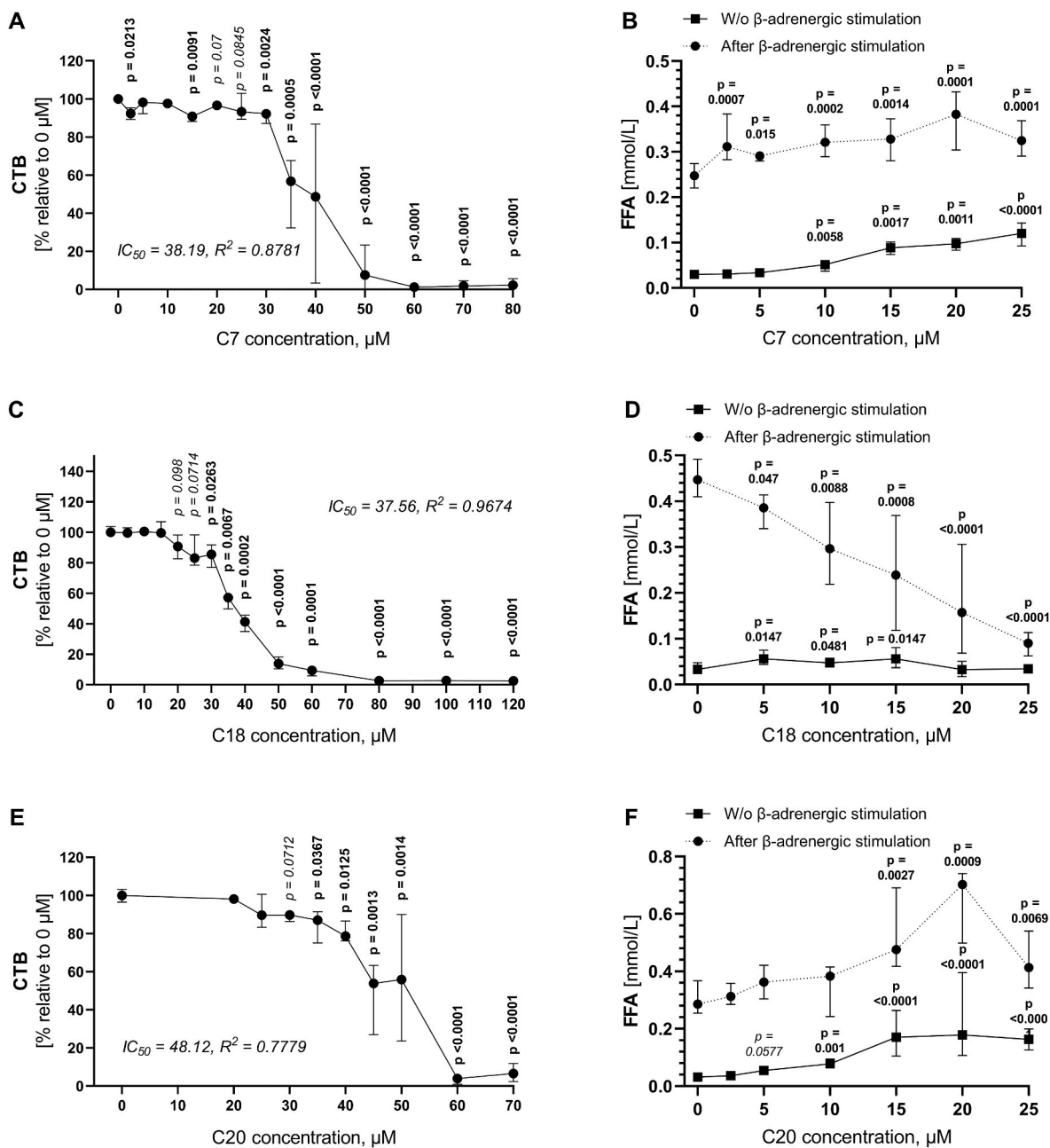


**Fig. 1.** Cytotoxic and lipolysis-modulating effects of the tested compounds in the model of differentiated 3T3-L1 adipocytes. CTB viability assay of 3T3-L1 cells treated for 24 h with compounds 7 (A), 18 (C), and 20 (E). FFAs (free fatty acids) released from 3T3-L1 cells treated for 24 h with compounds 7 (B), 18 (D), and 20 (F) with or without  $\beta$ -adrenergic stimulation according to the described protocol. Data are presented as Median  $\pm$  Interquartile range.

(from 0  $\mu$ M up to 25  $\mu$ M) that do not noticeably affect cell functions to assess the effects of compounds on the lipolysis rate. Paradoxically, all the tested molecules demonstrated pro-lipolytic action after 24 h of incubation (including 4 h in serum-starved medium), resulting in amplified release of free fatty acids (FFAs) (Fig. 1 B, D, F). This was contrary to the hypothesized suppression of lipolysis expected in the case of ERK3 inhibition [19] and raised questions about the ERK3-dependent inhibitory mechanisms of these compounds' action.

Considering that  $\beta$ -adrenergic regulation is crucial for lipolysis activation as well as for the pro-lipolytic action of ERK3 [19], we examined the effects of the substances under conditions of administration of the  $\beta$ -adrenergic ( $\beta_1$ ,  $\beta_2$ ,  $\beta_3$ ) agonist isoproterenol, which was added in the last 2 h of the experiment (Fig. 1 B, D, F) [31,32]. The treatment with two out of three molecules (C7 and C20) again led to the intensification of FFAs release, enhancing the lipolytic stimulation by

isoproterenol. However, C18 administration limited isoproterenol-stimulated lipolysis and resulted in a linear decrease in FFAs release below the control values.

Taken together, these data cast doubt on the ERK3-inhibition properties of C7 and C20, while the biological effects of C18 were found to be ambivalent. However, although the substances did not meet our expectations, their binding abilities to the ERK3 protein were previously confirmed in multiple tests [2]. Therefore, our next aim was to verify if the compounds' effects are selective and ERK3-dependent.

### 3.2. The effects of the studied substances are mostly ERK3-independent

To address the question of the selectivity of the action of the studied compounds, we decided to repeat the experiment on 3T3-L1 adipocytes transfected with *Erk3* shRNA for long-term *Erk3* gene silencing (shERK3)

and non-targeting control shRNA (shNTC) as a control. We hypothesized that if the tested molecules require ERK3 for its action, then the absence of ERK3 will not allow the substances to demonstrate their effects (or at least will reduce the severity of the effects).

In general, the direction of the effects previously demonstrated in non-transfected cells was preserved. Furthermore, ERK3 silencing upon  $\beta$ -adrenergic stimulation decreased the lipolysis rate, confirming previous results obtained by El-Merahbi et al. (Fig. 2 G) [19]. In this context, C7 and C20 showed ERK3-independent pro-lipolytic activity (Fig. 2 A, E), as also demonstrated in the previous experiment. It's worth noting that the effect of C7 was significantly lower in the absence of ERK3 (Fig. 2 B), suggesting a partial involvement of this kinase in the mechanism of the compound's action. Meanwhile, there was no difference in FFAs release between the shERK3 and shNTC groups after C20 treatment (Fig. 2 F). The activity of C18 in isoproterenol-stimulated conditions was also consistent with the results previously observed in non-transfected 3T3-L1 adipocytes (Fig. 2 C). However, the severity of the effect was similar with or without ERK3 silencing (Fig. 2 D).

Based on these data, we assume that the lipolysis-modulating effects of the studied substances are mostly ERK3-independent. However, to gain a final understanding of the mechanisms of their action, it's worth investigating the molecular changes associated with the regulation of lipolysis, especially considering the partial involvement of ERK3 in C7's pro-lipolytic activity and the anti-lipolytic effects of C18, which align with the hypothesized ones.

### 3.3. Tested compounds do not affect lipolysis-regulating proteins

Using isoproterenol-stimulated 3T3-L1 adipocytes, we examined protein levels of ERK3 and its downstream substrate MK5, together with the main lipolysis-driving enzymes: adipose triglyceride lipase (ATGL), hormone-sensitive lipase (HSL), and monoglyceride lipase (MGL) [31, 32]. Since we have demonstrated changes in FFAs levels upon the action of the compounds, we also assessed fatty acid synthase (FASN) as a marker of *de novo* fatty acid synthesis [33]. Considering the importance of protein kinase A (PKA) in the activation of lipolysis as well as its role in  $\beta$ -adrenergic-induced ERK3 stabilization, we also examined the protein levels of its catalytic subunit  $\alpha$  (PKA $\alpha$ ) [19,31,32].

The transfection of 3T3-L1 adipocytes with *Erk3* shRNA was successful and led to the evident absence of ERK3 protein, as shown in Fig. 3 A. Consistently, ERK3 silencing resulted not only in the reduction of ERK3 levels but also in the decreased abundance of MK5 [18,19]. In agreement with previously published data [19], the absence of ERK3 was accompanied by the decline of ATGL as well as the decrease of other lipolytic enzymes (HSL, MGL), and, paradoxically, of lipogenic enzyme FASN (Fig. 3 A). Additionally, we observed a diminution of PKA $\alpha$ , which was not previously reported to our knowledge.

Surprisingly, treating adipocytes with each studied compound in the presence of  $\beta$ -adrenergic stimulation also resulted in the reduction of ERK3 protein levels (Fig. 3 B–D). It is known that ERK3 is a highly unstable protein that is rapidly and constitutively degraded in proliferating cells with a half-life of 30 min [5,8]. Ser<sup>189</sup> phosphorylation in the ERK3 activation loop is required for the kinase to form a stable complex with MK5, protecting both enzymes from degradation [1,19]. Moreover, ERK3 phosphorylation itself is linked to the stabilization of the kinase [6]. Based on the proven binding abilities of the tested molecules to ERK3, which rule out its phosphorylation on Ser<sup>189</sup> and impact on MK5 recognition [2], we propose that the introduction of the compounds leads to the failure of ERK3/MK5 complex formation, thus ultimately promoting kinases degradation. The decline of MK5 levels after C7 and C20 treatment indirectly confirms this hypothesis (Fig. 3 B, D). Moreover, conformational and probable phosphorylation changes due to compound-kinase interactions can also make ERK3 more prone to accelerated ubiquitin-proteasome degradation [5,8]. Besides, the reduction in ERK3 abundance may be due to off-target effects of the compounds on another kinase(s) that regulate ERK3 degradation.

Despite ERK3 and MK5 depletion, the tested molecules did not affect levels of any other lipolysis-regulating proteins studied in the current research, demonstrating a different molecular pattern compared to the silencing of ERK3 (Fig. 3). The observed reduction in target protein levels, as well as some other effects (e.g., proliferative and anti-lipolytic effects of C18 consistent with those hypothesized, a significant reduction in C7 effects in the absence of the kinase, etc.), coupled with the high binding and inhibitory properties demonstrated by Grädler et al. [2], may indicate that the selected compounds inhibit ERK3 *in vivo*. However, the rest of the data (including the altered molecular pattern revealed in western blotting and predominantly pro-lipolytic effects in most of the conditions) suggest that the biological effect of this inhibition is significantly overlapped and modified by some other molecular events, probably related to the non-selective binding of the substances to other targets. It's important to note that such a possibility was also considered by the authors of the original paper (Fig. 4 A) [2].

### 3.4. Machine learning-based prediction revealed a wide range of possible targets for the tested compounds

During the initial characterization of the proposed substances, it was acknowledged that they may not exhibit absolute selectivity against ERK3. For example, it was shown that C18 has additional kinase-inhibiting activity (above 80 % at 1  $\mu$ M) with EIF2AK4 (eIF-2-alpha kinase GCN2) and GSK3A (Glycogen synthase kinase-3 alpha) based on a kinase selectivity screen (KINOMEScan™, DiscoverX, DX). Moreover, the C20 kinase selectivity profile demonstrated an even greater number of potential targets: 29 out of 389 kinases were inhibited above 80 % at 1  $\mu$ M (Fig. 4 A).

Regrettably, the data presented by Grädler et al. did not include the C7 kinase selectivity profile [2]. Besides, the screening considered only kinases as potential targets but did not assess possible interactions of the compounds with other biologically active substances, receptors, etc. That is why we decided to perform a broader screening by applying a machine learning-based approach using the SuperPred 3.0 platform (publicly available at [https://prediction.charite.de/subpages/target\\_prediction.php](https://prediction.charite.de/subpages/target_prediction.php)) [34]. The dataset for the target prediction was obtained from the ChEMBL database and resulted in 500,979 unique trusted relations between 365,719 strongly binding substances and 2353 targets. The authors declare one of the best prediction levels of SuperPred 3.0 compared to other recent publications [34].

Based on the SuperPred 3.0 screen, potential targets with more than a 90 % binding probability for at least one of the tested molecules included 26 proteins encoded by the following genes: *NFKB1*, *FAAH*, *PTGS1*, *KDM1A*, *CDK2*, *CDK4*, *MAPK9*, *CLK1*, *DUSP3*, *ALOX12*, *CDK1*, *NTRK3*, *NPC1*, *HIF1A*, *PTK2B*, *KCNH2*, *MAPK10*, *CXCR4*, *FASN*, *APEX1*, *AURKB*, *CHUK*, *GPBAR1*, *CREBBP* (Fig. 4 B). This gives us an additional reason to believe that the studied substances can bind not only to ERK3 but also to a wide range of targets with extensive biological effects.

### 3.5. Compounds reaffirm pro-lipolytic effects in primary adipocytes

To confirm and verify the metabolic effects of the selected compounds observed in a stable cell line, we decided to use a more physiological model of adipocytes derived from primary stromal vascular cells (SVCs). This is especially reasonable since the impact of ERK3 inactivation is dependent on the cellular context [4], and the role of ERK3 is cell-type dependent [35,36].

We began with another round of screening for the cytotoxic effects of the substances in the new model. Since both enzymatic tests used in the previous experimental series generally showed similar results, and considering some disadvantages of MTT (such as its cytotoxic effect on examined cells, an additional dissolving step in the procedure, and the possibility to interfere with other substances, etc. [25–28]), we decided to limit ourselves to using only CTB and crystal violet assays.

As predicted, the results of cytotoxicity assays in this model were

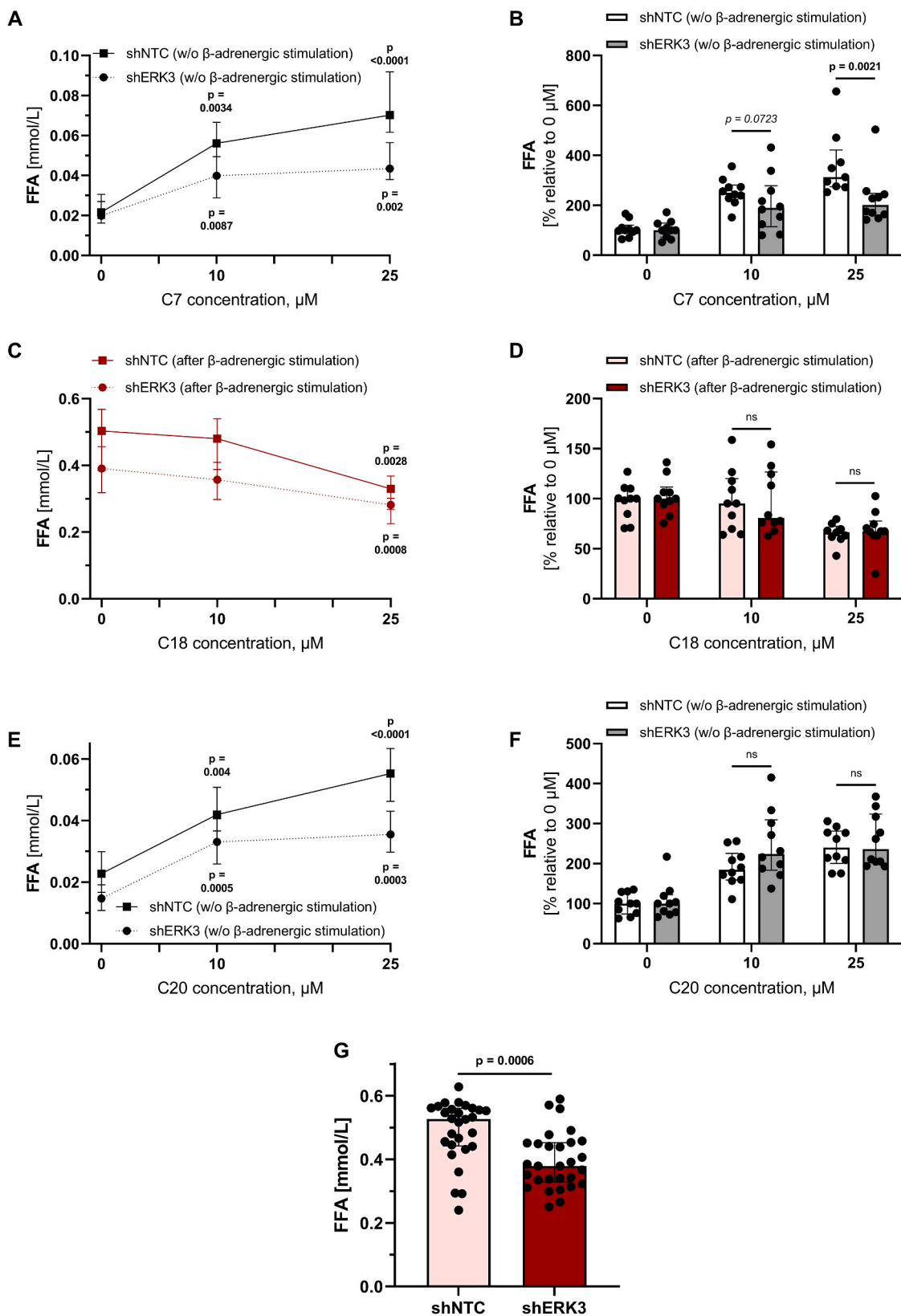


**Fig. 2.** ERK3-independent nature of the metabolic effects of the studied compounds. **In the right panel**, FFAs (free fatty acids) released from *Erk3* shRNA-transfected 3T3-L1 adipocytes and control (NTC) cells treated for 24 h with compounds 7 (A), 18 (C), and 20 (E) in the presence of  $\beta$ -adrenergic stimulation (C) or without it (A, E). **In the left panel**, the impact of *Erk3* silencing on the severity of the effects of compounds 7 (B), 18 (C), and 20 (F) in the presence of  $\beta$ -adrenergic stimulation (C) or without it (B, F) relative to a particular control group (shERK3 or shNTC). ERK3 silencing upon  $\beta$ -adrenergic stimulation decreases the lipolysis rate (G): FFAs released from shERK3 and shNTC adipocytes after  $\beta$ -adrenergic stimulation without compound treatment (data are obtained from the pooling of the respective control groups (shERK3 and shNTC) used in the current study). Data are presented as Median  $\pm$  Interquartile range. The color red was used to indicate experimental conditions accompanied by stimulation with a  $\beta$ -agonist according to the described protocol.

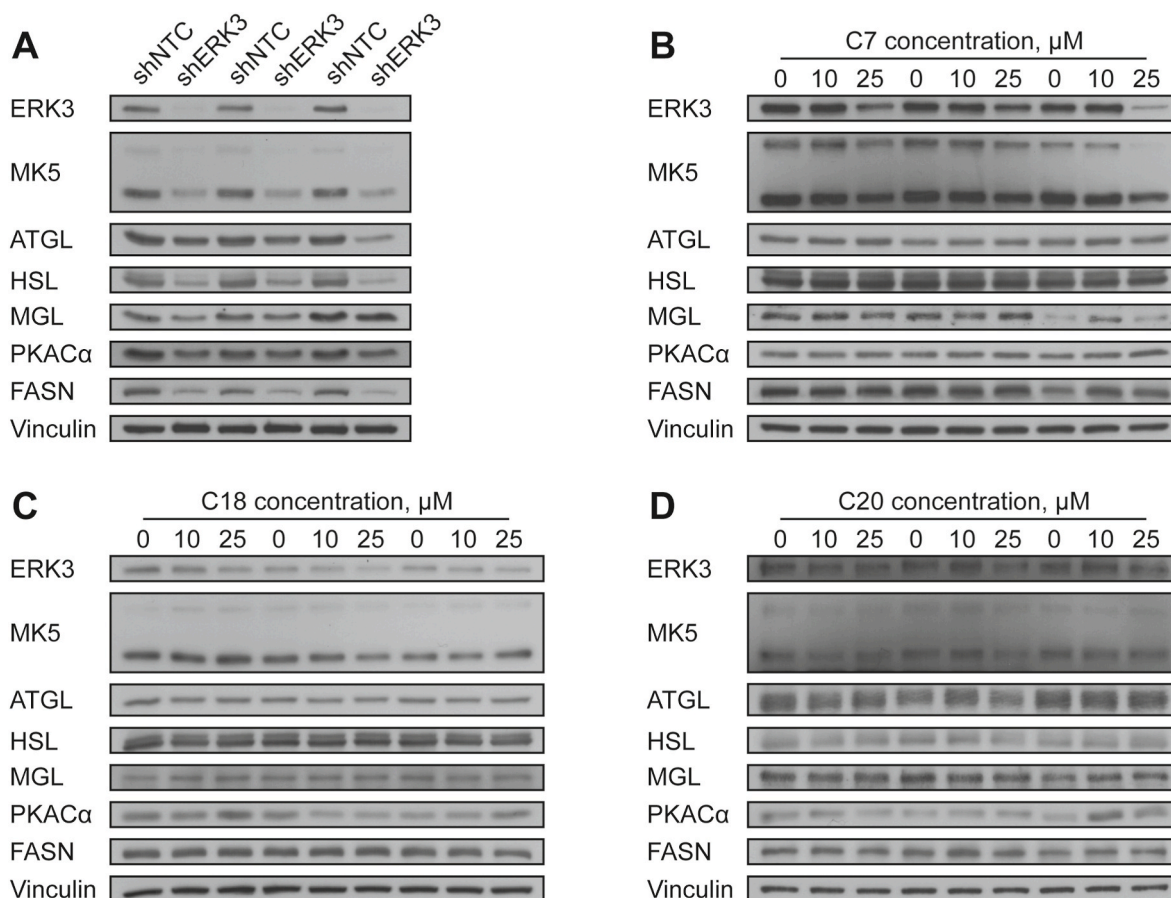


**Fig. 3.** *Erk3* silencing inhibits protein levels of protein kinase A (PKA) along with the main lipolytic enzymes, while compounds do not demonstrate this pattern of activity. (A) Western blot analysis for ERK3, MK5, ATGL, HSL, MGL, FASN, and PKAC $\alpha$  proteins in differentiated 3T3-L1 cells transfected with *Erk3* shRNA and control cells stimulated for 2 h with isoproterenol according to the protocol (number of independent repetitions = 3). Western blot analysis for selected proteins in differentiated 3T3-L1 cells stimulated for 2 h with isoproterenol according to the protocol and treated with C7 (B), C18 (C), or C20 (D) (number of independent repetitions = 3).

slightly different from those for 3T3-L1 cells (Fig. 5 A, C, E, Fig. S32). First of all, in the model of primary adipocytes, both enzymatic and non-enzymatic assays showed very consistent values. Additionally, all compounds demonstrated a more pronounced inhibition of adipocytes' viability at lower doses. The average CVS/CTB IC<sub>50</sub> for all studied molecules was approximately 29  $\mu$ M, which was almost 40 % lower compared to 3T3-L1 cells. Furthermore, the level of this effect was much more variable between the tested molecules, with the highest toxicity noted for C7 (average CVS/CTB IC<sub>50</sub> = 21.59  $\mu$ M) and the lowest toxicity noted for C20 (average CVS/CTB IC<sub>50</sub> = 37.74  $\mu$ M). C18 showed a moderate level of toxicity compared to other molecules (average CVS/CTB IC<sub>50</sub> = 26.60  $\mu$ M). It's interesting to note that we once again observed an upward trend in the crystal violet values after treating adipocytes with low concentrations of C18, serving as indirect evidence of ERK3 inhibition. However, this effect was not statistically significant.

Based on the individual compound's cytotoxicity, we selected "safe" doses to assess the metabolic effects of the molecules. In agreement with the altered viability, the lipolysis-modulating effects of the studied compounds were also slightly modified in the SVC model (Fig. 5 B, D, F). Although the general direction of the effects was consistent with the previously observed results, we didn't find any influence on isoproterenol-stimulated lipolysis, as the levels of FFAs steadily increased compared to unstimulated conditions but were not affected by any treatment. However, in isoproterenol-free conditions, we observed the same trend as seen in 3T3-L1 cells — amplified FFAs release after 24 h. As in a stable cell line, this effect was present at all doses of all substances used on primary adipocytes. All of this is consistent with the data

that, on the one hand, 3T3-L1 and primary cells share great overlap at the proteome level, but, on the other hand, they also have significant differences in several pathways intrinsic to adipocyte biology, such as fatty acid and glycerolipid metabolism [37].

Considering the results obtained from two independent adipocyte models, we conclude that the biological effects of the selected compounds tend to be pro-lipolytic. These effects do not appear to be related to ERK3-dependent inhibition, as they oppose the ones observed after selective ERK3 silencing [18,19]. Based on the current research, we assert that despite the high binding affinity and potency of the tested compounds, they are unable to selectively inhibit ERK3 in adipocytes.

#### 4. Discussion and perspectives

ERK3 is a ubiquitously expressed kinase participating in the regulation of a wide spectrum of physiological processes [4–8]. Targeted inhibition of the kinase may allow the development of new treatment strategies for a variety types of cancer and somatic pathologies, as well as for preserving metabolic health and combating obesity and diabetes [9–19]. However, there are currently no available substances with proven specific and selective ERK3-inhibiting properties [2,5,20,21]. We chose and synthesized three compounds with the most attractive properties proposed by Grädler et al. as novel ERK3 inhibitors [2] to assess their selectivity and biological effects in living cells in terms of their impact on metabolic state.

Using different adipocyte models, we demonstrated that two molecules (C7 and C20) unexpectedly exhibit a persistent pro-lipolytic effect,

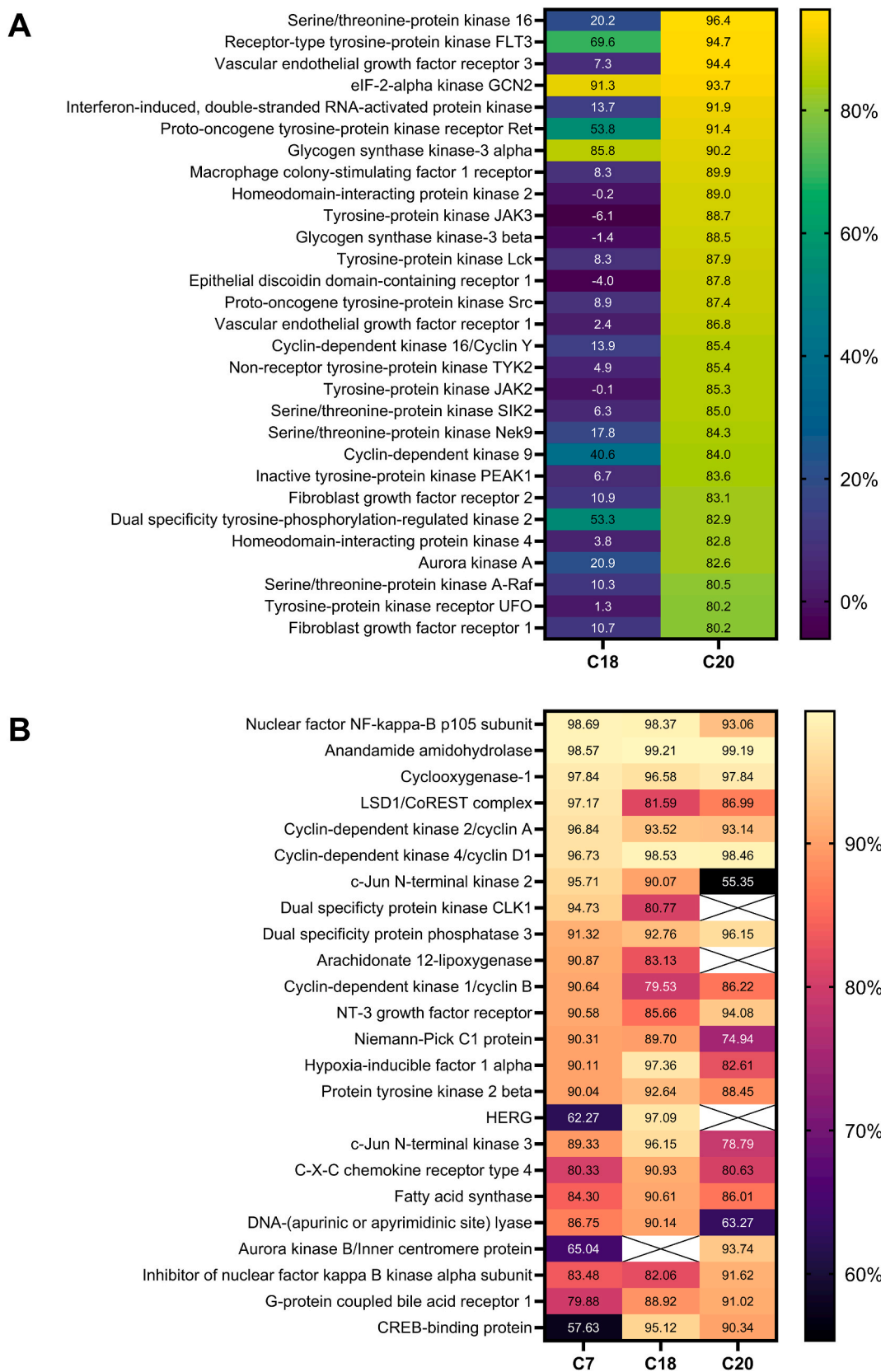


**Fig. 4.** Tested compounds may have other targets different from ERK3. (A) Kinase selectivity profile (KINOMEScan™, DiscoverX, DX) of C18 and C20, indicating kinases inhibited above 80 % at 1  $\mu$ M [published by Grädler et al., 2020] (data presented as % of inhibition at 1  $\mu$ M). (B) Results of compounds' target prediction using SuperPred 3.0, listing proteins with more than 90 % binding probability for at least one of the tested molecules (data presented as % of the probability).

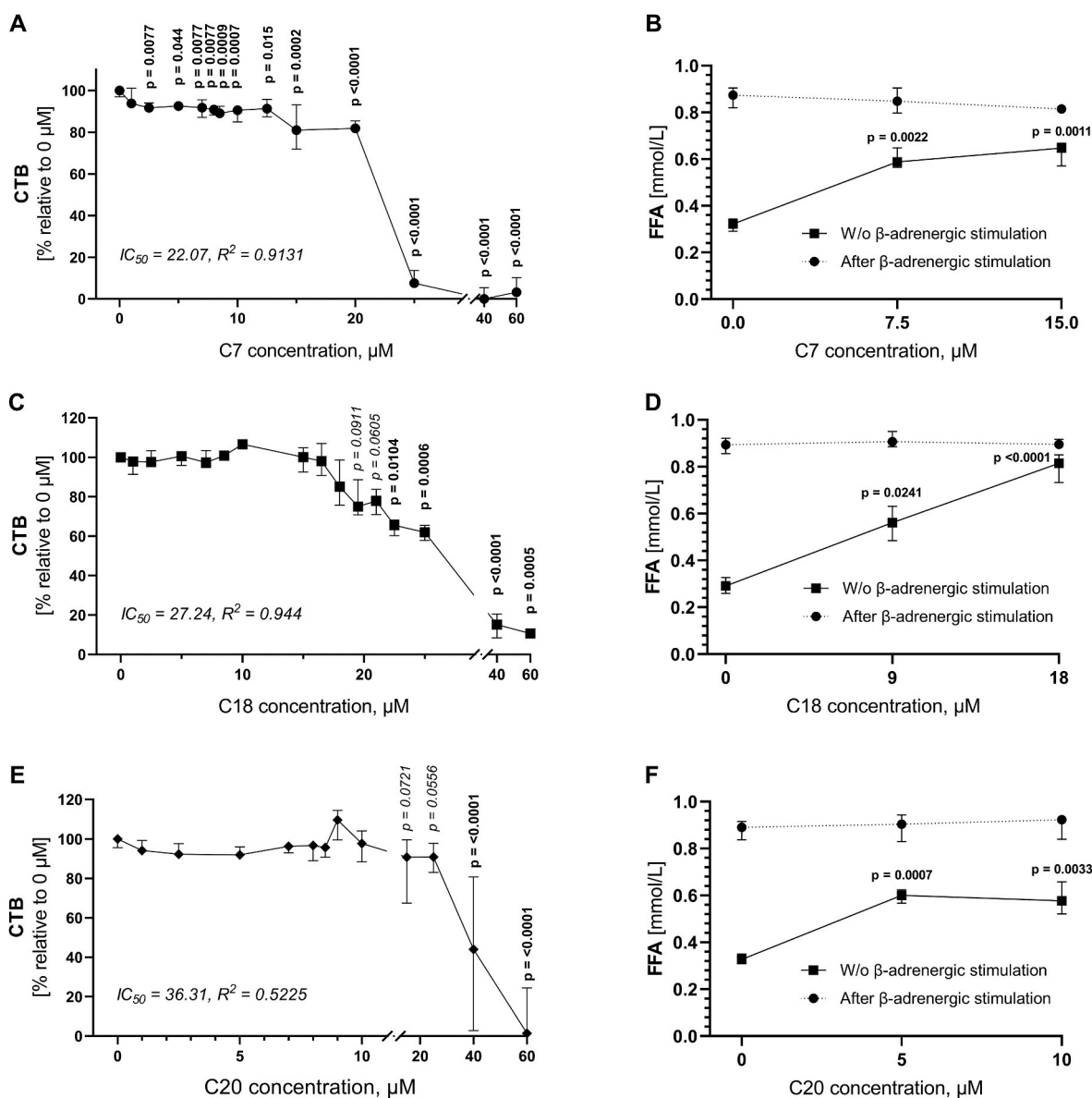


**Fig. 5.** Cytotoxic and pro-lipolytic effects of the studied compounds in the model of primary stromal-vascular cell (SVC)-derived adipocytes. CTB viability assay of primary adipocytes treated for 24 h with compounds 7 (A), 18 (C), and 20 (E). FFAs (free fatty acids) released from SVCs treated for 24 h with compounds 7 (B), 18 (D), and 20 (F) with or without  $\beta$ -adrenergic stimulation according to the described protocol. Data are presented as Median  $\pm$  Interquartile range.

while C18's action is ambivalent: anti-lipolytic in  $\beta$ -adrenergic-induced conditions and pro-lipolytic without stimulation. Overall, this type of cellular response is inconsistent with the assumption of selective ERK3 inhibition suppressing fatty acid output [18,19] and implies the involvement of some other mechanisms. Further studies on ERK3-silenced adipocytes also demonstrated mostly kinase-independent effects of the tested substances. In addition, the administration of compounds did not affect the levels of the lipolysis-regulating proteins, exhibiting a different molecular pattern compared to the ERK3-selective knockdown. However, the inhibition of ERK3 and MK5 protein levels upon treatment was revealed. Of note, a few events (C18-dependent stimulation of cell proliferation as well as its anti-lipolytic effect and the weakening of the effects of C7 in the absence of ERK3) also suggest at least partial involvement of ERK3 in the mechanism of the compounds' action [5,7,8,30].

Based on the results of our study as well as the initial profiling done by Grädler et al., we suggest that the tested compounds are capable of inhibiting ERK3 *in vitro*. However, the biological effect of this inhibition is significantly overlapped and modified by some other molecular events

related to the non-selective binding to other targets. Besides, the lack of substantial manifestations of ERK3 inhibition, aside from the compounds' influence on other targets, may be related to the suggested possible redundancy between closely related ERK3 and ERK4 protein kinases [1]. Subsequently, we revealed a wide range of the compounds' possible targets using a machine learning-based prediction.

Another result of this study was the expansion of knowledge about the features of ERK3 signaling and its biological effects. Special attention should be paid to the discovered reduction not only of lipolytic enzymes (such as ATGL, HSL, and MGL) but, paradoxically, also of the lipogenic ones (FASN) observed upon ERK3 silencing. Together with the decline of PKAC $\alpha$ , this requires further investigation due to its high physiological importance.

To obtain these results, various methods and models were utilized, and certain differences and nuances merit separate discussion. Below, we provide justification for the selection of viability assays. The MTT and CTB assays are based on non-specific cellular metabolic activity, resulting in the reduction of the respective indicators (tetrazolium to formazan, or resazurin to resorufin, respectively) [26,27]. It has been

shown that tetrazolium is reduced by FMNH<sub>2</sub>, FADH<sub>2</sub>, NADH, NADPH, succinate and lactate dehydrogenases, peroxidases, etc., resulting in the shutdown of the biological respiratory chain. In contrast, resazurin is also reduced by the cytochromes, but it requires increased redox potential for reduction reactions and maintains the function of the respiratory chain compared to the MTT [25–28]. Another notable distinction is that resorufin, being cell membrane-permeable, can to spread in the medium, slightly affecting basal metabolism, while formazan is water-insoluble, so its crystals are formed and accumulated intracellularly, leading to cell death [28]. MTT and CTB assays are complementary techniques to measure cell survival after drug treatment [26]. However, it's important to note that these enzymatic tests do not assess the viability of cells but rather report on aspects of metabolic activity, dysfunction, or impairment [29]. A simple, metabolism-independent, non-enzymatic assay used in the present study that avoids the limitations undermining the accuracy of the enzymatic assays is the crystal violet staining. This method leverages the interaction between the dye and the external surface of the DNA double helix, permitting the estimation of the number of viable cells [25]. Subsequently, we decided to restrict ourselves to using only two assays, as MTT generally yielded similar results to CTB, while also considering some of its drawbacks (its own cytotoxic effect on examined cells, an additional dissolving step in the procedure, the possibility to interfere with other substances, etc. [25–28]).

At the moment, we found a single published research using one of the tested molecules (C18) in living cells [4]. However, the authors did not aim to study the biological effects and selectivity of the compound, and they applied it, among other methods, only to validate the impact of ERK3 on its newly discovered substrate supervillin (SVIL). So, there was a limited amount of information published. In general, the effect of C18 was in line with what was expected from ERK3 deletion, and it led to the reduced phosphorylation of SVIL, as well as an increased frequency of multinucleated cells. This is consistent with and confirms our assertion about the ERK3-inhibiting properties of the compound. Nevertheless, it should be pointed out that upon C18 treatment, the decrease in ERK3 protein level observed in our study wasn't noticed. This can probably be explained by the lower concentration of C18 used (only 5  $\mu$ M vs. 10  $\mu$ M and 25  $\mu$ M in the current research), as well as a different type of cells (Hs578T breast cancer cells vs. 3T3-L1 adipocytes).

It is important to note that the substances occasionally exhibited not only linear (dose-dependent) but also so-called bell-shaped dose-response curves (e.g., see Fig. 1, Fig. S31), which are also observed when targeting different kinases [38–40]. At the same time, the effects of ERK3 themselves are sometimes not quite clear. For instance, despite the cancer-promoting effects of ERK3 noted above, there are a few studies demonstrating kinase-dependent inhibition of cell proliferation in multiple cancer cell lines, including squamous cell carcinoma, hepatocarcinoma, and melanoma [35,36,41], or even an absence of impact on cancer cell growth [35,36]. This means that the role of ERK3 is highly dependent on the cellular context and cell type [4,35,36].

We speculate that the observed increase in the lipolysis rate could occur upon compounds' interaction with some of the members of the cyclin-dependent kinases (CDKs) family, which are able to directly regulate metabolic enzymes and target metabolic regulators [42]. They are widely represented among potential targets according to both SuperPred 3.0 prediction and the kinase selectivity screen (Fig. 4). For instance, such a target could be cyclin-dependent kinase 4/cyclin D1, which is essential for promoting anabolic and suppressing catabolic metabolism in adipocytes [42,43]. It's also interesting that the interaction of ERK3 with cyclin B-CDK1 and cyclin D3 was shown previously [4, 6]. However, it is important to note that the list of potential targets that can modulate lipid metabolism is not limited to CDKs but also includes eIF-2-alpha kinase GCN2 [44], glycogen synthase kinase-3 alpha [45], anandamide amidohydrolase [46], etc. At the same time, it is obvious that modern methods for predicting the functions of new molecules still have significant shortcomings that require confirmation of the effects *in*

*vivo*. Curiously, FASN, one of the targets from the prediction list, was assessed in the current research; however, compounds didn't impact it. Moreover, there was surprisingly no ERK3 among the potential targets (Fig. 4 B). Thus, the *in-silico* prediction of ERK3 off-targets has limited value in the absence of follow-up validation assays. Nevertheless, the search and verification of the tested molecules' targets were beyond the scope of this study.

Despite the fact that the substances did not meet our expectations in the context of correcting metabolic disorders, there may still be relevance in their study. First of all, the studied molecules are of practical interest for the development of polyfunctional multi-target drugs with antitumor effects, given that the components can affect not only ERK3 but also other potential targets, many of which are already used or are being considered for use in cancer therapy (e.g., the mentioned CDKs) [20,47]. Moreover, triazole-fused pyrimidines, substances with a similar chemical structure, have already attracted considerable interest as potential anticancer agents that direct various cancer-associated targets (including tubulin, polycomb repressive complex 2 (PRC2), PI3K/mTOR, different tyrosine kinases, etc.) in recent years [20]. In addition, the study of tested molecules has the potential to contribute to the discovery of new ERK3 regulators, as well as a better understanding of the biological effects and mechanisms of ERK3 signaling.

Thus, for the first time, ERK3 was found to promote the abundance of HSL, MGL, FASN, as well as PKA $\alpha$  in adipocytes. In addition, the novelty of the study was the investigation of the selectivity of the action as well as the biological effects of the triazolo [4,5-*d*]pyrimidin-5-amines based ERK3 inhibitors in living cells. It was shown that compounds exhibit lipolysis-modulating effects, although this influence on adipocyte function is not dependent on ERK3.

## 5. Author contributions

Conceptualization, A.B., I.H. and G.S.; data curation, A.B., K.K.-M. and G.S.; formal analysis, A.B., K.K.-M., A.L.-V., A.M. and G.S.; validation, A.B., K.K.-M. and G.S.; investigation, A.B. and A.M.; visualization & writing—original draft, A.B.; methodology, A.B., I.H., K.K.-M., A.L.-V., A.M. and G.S.; project administration & resources, G.S. and A.M.; writing—review and editing, funding acquisition & supervision, G.S.

## Funding

The study was funded by the National Science Centre, Poland (Sonata Bis 10, grant no. 2020/38/E/NZ4/00314) and by the Dioscuri Centre of Scientific Excellence — a program initiated by the Max Planck Society, managed jointly with the National Science Centre in Poland, and mutually funded by Polish Ministry of Science and German Federal Ministry of Education and Research.

## Conflict of interest

The authors have declared that no conflict of interest exists.

## Data availability

The source data reported in this paper have been archived in the Open Science Framework (OSF) repository (DOI: 10.17605/OSF.IO/G7XUC). These data are publicly accessible at <https://osf.io/g7xuc/>.

## Declaration of competing interest

The authors have declared that no conflict of interest exists.

## Acknowledgments

We thank Jacek Olędzki Ms.C. (Institute of Biochemistry and Biophysics, PAS) for recording the ES-MS spectra and Marcin Wilczek

Ph.D. (Department of Chemistry, University of Warsaw) for acquiring and supporting in interpreting of NMR spectra.

## Appendix A. Supplementary data

Supplementary data to this article can be found online at <https://doi.org/10.1016/j.abb.2023.109825>.

## References

- [1] N. Ronkina, M. Gaestel, MAPK-activated protein kinases: servant or partner? *Annu. Rev. Biochem.* 91 (2022) 505–540, <https://doi.org/10.1146/annurev-biochem-081720-114505>.
- [2] U. Grädler, M. Busch, B. Leuthner, M. Raba, L. Burgdorf, M. Lehmann, N. Linde, C. Esdar, Biochemical, cellular and structural characterization of novel and selective ERK3 inhibitors, *Bioorg. Med. Chem. Lett* 30 (2020), 127551, <https://doi.org/10.1016/j.bmcl.2020.127551>.
- [3] T. Kassouf, G. Sumara, Impact of conventional and atypical MAPKs on the development of metabolic diseases, *Biomolecules* 10 (2020) 1256, <https://doi.org/10.3390/biom10091256>.
- [4] J. Javary, E. Goupil, M. Soulez, E. Kanshin, A. Bouchard, O. Seternes, P. Thibault, J. Labbé, S. Meloche, Phosphoproteomic analysis identifies supervillin as an ERK3 substrate regulating cytokinesis and cell ploidy, *J. Cell. Physiol.* (2022), <https://doi.org/10.1002/jcp.30938>.
- [5] M. Cargnello, P.P. Roux, Activation and function of the MAPKs and their substrates, the MAPK-activated protein kinases, *Microbiol. Mol. Biol. Rev.* 75 (2011) 50–83, <https://doi.org/10.1128/MMBR.00031-10>.
- [6] P.-L. Tanguay, G. Rodier, S. Meloche, C-terminal domain phosphorylation of ERK3 controlled by Cdk1 and Cdk14 regulates its stability in mitosis, *Biochem. J.* 428 (2010) 103–111, <https://doi.org/10.1042/BJ20091604>.
- [7] C. Julien, P. Coulombe, S. Meloche, Nuclear export of ERK3 by a CRM1-dependent mechanism regulates its inhibitory action on cell cycle progression, *J. Biol. Chem.* 278 (2003) 42615–42624, <https://doi.org/10.1074/jbc.M302724200>.
- [8] P. Coulombe, G. Rodier, S. Pelletier, J. Pellerin, S. Meloche, Rapid turnover of extracellular signal-regulated kinase 3 by the ubiquitin-proteasome pathway defines a novel paradigm of mitogen-activated protein kinase regulation during cellular differentiation, *Mol. Cell Biol.* 23 (2003) 4542–4558, <https://doi.org/10.1128/MCB.23.13.4542-4558.2003>.
- [9] Q. Cai, W. Zhou, W. Wang, B. Dong, D. Han, T. Shen, C.J. Creighton, D.D. Moore, F. Yang, MAPK6-AKT signaling promotes tumor growth and resistance to mTOR kinase blockade, *Sci. Adv.* 7 (2021), eabi6439, <https://doi.org/10.1126/sciadv.abi6439>.
- [10] J. Wu, Y. Zhao, F. Li, B. Qiao, MIR-144-3p: a novel tumor suppressor targeting MAPK6 in cervical cancer, *J. Physiol. Biochem.* 75 (2019) 143–152, <https://doi.org/10.1007/s13105-019-00681-9>.
- [11] M. Zhang, H. Wang, X. Zhang, F. Liu, miR-653-5p suppresses the growth and migration of breast cancer cells by targeting MAPK6, *Mol. Med. Rep.* 23 (2021) 200, <https://doi.org/10.3892/mmr.2021.11839>.
- [12] K. Bogucka, M. Pompaiah, F. Marini, H. Binder, G. Harms, M. Kaulich, M. Klein, C. Michel, M.P. Radsak, S. Rosigkeit, P. Grimminger, H. Schild, K. Rajalingam, ERK3/MAPK6 controls IL-8 production and chemotaxis, *Elife* 9 (2020), e52511, <https://doi.org/10.7554/eLife.52511>.
- [13] W. Long, C.E. Foulds, J. Qin, J. Liu, C. Ding, D.M. Lonard, L.M. Solis, I.I. Wistuba, J. Qin, S.Y. Tsai, M.-J. Tsai, B.W. O'Malley, ERK3 signals through SRC-3 coactivator to promote human lung cancer cell invasion, *J. Clin. Invest.* 122 (2012) 1869–1880, <https://doi.org/10.1172/JCI61492>.
- [14] K. Bogucka, F. Marini, S. Rosigkeit, J. Schloeder, H. Jonuleit, K. David, M. Schlackow, K. Rajalingam, ERK3/MAPK6 is required for KRAS-mediated NSCLC tumorigenesis, *Cancer Gene Ther.* 28 (2021) 359–374, <https://doi.org/10.1038/s41417-020-00245-w>.
- [15] T. Yao, D. Zha, C. Hu, X. Wu, Circ\_0000285 promotes podocyte injury through sponging miR-654-3p and activating MAPK6 in diabetic nephropathy, *Gene* 747 (2020), 144661, <https://doi.org/10.1016/j.gene.2020.144661>.
- [16] M. Liang, D. Zhang, D. Zheng, W. He, J. Jin, Exosomes from miR-374a-5p-modified mesenchymal stem cells inhibit the progression of renal fibrosis by regulating MAPK6/MK5/YAP axis, *Bioengineered* 13 (2022) 4517–4527, <https://doi.org/10.1080/21655979.2022.2033465>.
- [17] Z.-Q. Huang, W. Xu, J.-L. Wu, X. Lu, X.-M. Chen, MicroRNA-374a protects against myocardial ischemia-reperfusion injury in mice by targeting the MAPK6 pathway, *Life Sci.* 232 (2019), 116619, <https://doi.org/10.1016/j.lfs.2019.116619>.
- [18] A. Loza-Valdes, R. El-Merabhi, T. Kassouf, A. Demczuk, S. Reuter, J.T. Viera, T. Karwen, M. Noh, M.C. Löffler, R. Romero-Becerra, J.L. Torres, M. Marcos, G. Sabio, U. Wojda, G. Sumara, Targeting ERK3/MK5 complex for treatment of obesity and diabetes, *Biochem. Biophys. Res. Commun.* 612 (2022) 119–125, <https://doi.org/10.1016/j.bbrc.2022.04.070>.
- [19] R. El-Merabhi, J.T. Viera, A.L. Valdes, K. Koczynska, S. Reuter, M.C. Löffler, M. Erk, C.P. Ade, T. Karwen, A.E. Mayer, M. Eilers, G. Sumara, The adrenergic-induced ERK3 pathway drives lipolysis and suppresses energy dissipation, *Genes Dev.* 34 (2020) 495–510, <https://doi.org/10.1101/gad.333617.119>.
- [20] X.-J. Dai, L.-P. Xue, S.-K. Ji, Y. Zhou, Y. Gao, Y.-C. Zheng, H.-M. Liu, H.-M. Liu, Triazole-fused pyrimidines in target-based anticancer drug discovery, *Eur. J. Med. Chem.* 249 (2023), 115101, <https://doi.org/10.1016/j.ejmech.2023.115101>.
- [21] M. Schröder, P. Filippakopoulos, M.P. Schwalm, C.A. Ferrer, D.H. Drewry, S. Knapp, A. Chaikwad, Crystal structure and inhibitor identifications reveal targeting opportunity for the atypical MAPK kinase ERK3, *IJMS* 21 (2020) 7953, <https://doi.org/10.3390/ijms21217953>.
- [22] D. Dorsch, G. Hoelzemann, M. Calderini, A. Wegener, O. Poeschke, Triazololo[4,5-d]pyrimidine Derivatives for the Treatment of Diseases Such as Cancer, 2014, WO2014135244. <https://patentscope.wipo.int/search/en/detail.jsf?docId=WO2014135244>.
- [23] M. Perander, R. Al-Mahdi, T.C. Jensen, J.A.L. Nunn, H. Kildalsen, B. Johansen, M. Gabrielsen, S.M. Keyse, O.-M. Seternes, Regulation of atypical MAP kinases ERK3 and ERK4 by the phosphatase DUSP2, *Sci. Rep.* 7 (2017), 43471, <https://doi.org/10.1038/srep43471>.
- [24] M.C. Löffler, A.E. Mayer, J. Trujillo Viera, A. Loza Valdes, R. El-Merabhi, C.P. Ade, T. Karwen, W. Schmitz, A. Slotta, M. Erk, S. Janaki-Raman, N. Matesanz, J. L. Torres, M. Marcos, G. Sabio, M. Eilers, A. Schulze, G. Sumara, Protein kinase D1 deletion in adipocytes enhances energy dissipation and protects against adiposity, *EMBO J.* 37 (2018), e99182, <https://doi.org/10.15252/emboj.201899182>.
- [25] L. Śliwka, K. Wiktorska, P. Suchocki, M. Jilczarek, S. Mielczarek, K. Lubelska, T. Cierpiał, P. Łyżwa, P. Kielbasiński, A. Jaromin, A. Flis, Z. Chilmonczyk, The comparison of MTT and CVS assays for the assessment of anticancer agent interactions, *PLoS One* 11 (2016), e0155772, <https://doi.org/10.1371/journal.pone.0155772>.
- [26] E. Henriksson, E. Kjellén, P. Wahlberg, J. Wennerberg, J.H. Kjellström, Differences in estimates of cisplatin-induced cell kill in vitro between colorimetric and cell count/colony assays, *In Vitro Cell. Dev. Biol. Anim.* 42 (2006) 320–323, <https://doi.org/10.1290/0604022.1>.
- [27] B.H. Neufeld, J.B. Tapia, A. Lutzke, M.M. Reynolds, Small molecule interferences in resazurin and MTT-based metabolic assays in the absence of cells, *Anal. Chem.* 90 (2018) 6867–6876, <https://doi.org/10.1021/acs.analchem.8b01043>.
- [28] K. Präbst, H. Engelhardt, S. Ringgeler, H. Hübner, Basic colorimetric proliferation assays: MTT, WST, and resazurin, in: D.F. Gilbert, O. Friedrich (Eds.), *Cell Viability Assays*, Springer New York, New York, NY, 2017, pp. 1–17, [https://doi.org/10.1007/978-1-4939-6960-9\\_1](https://doi.org/10.1007/978-1-4939-6960-9_1).
- [29] B. Vieira-da-Silva, M.A.R.B. Castanho, Resazurin reduction-based assays revisited: guidelines for accurate reporting of relative differences on metabolic status, *Molecules* 28 (2023) 2283, <https://doi.org/10.3390/molecules28052283>.
- [30] Z. Xiang, S. Wang, Y. Xiang, Up-regulated MicroRNA499a by hepatitis B virus induced hepatocellular carcinogenesis via targeting MAPK6, *PLoS One* 9 (2014), e111410, <https://doi.org/10.1371/journal.pone.0111410>.
- [31] G.F. Grabner, H. Xie, M. Schweiger, R. Zechner, Lipolysis: cellular mechanisms for lipid mobilization from fat stores, *Nat. Metab.* 3 (2021) 1445–1465, <https://doi.org/10.1038/s42255-021-00493-6>.
- [32] E. London, M. Bloyd, C.A. Stratakis, PKA functions in metabolism and resistance to obesity: lessons from mouse and human studies, *J. Endocrinol.* 246 (2020) R51–R64.
- [33] D. Vanauberg, C. Schulz, T. Lefebvre, Involvement of the pro-oncogenic enzyme fatty acid synthase in the hallmarks of cancer: a promising target in anti-cancer therapies, *Oncogenesis* 12 (2023) 16, <https://doi.org/10.1038/s41389-023-00460-8>.
- [34] K. Gallo, A. Goede, R. Preissner, B.-O. Gohlke, SuperPred 3.0: drug classification and target prediction—a machine learning approach, *Nucleic Acids Res.* 50 (2022) W726–W731, <https://doi.org/10.1093/nar/gkac297>.
- [35] E.S. Alshammari, A.A. Aljaghtmi, A.J. Stacy, M. Bottomley, H.N. Shamma, M. P. Kadakia, W. Long, ERK3 is transcriptionally upregulated by ΔNp63α and mediates the role of ΔNp63α in suppressing cell migration in non-melanoma skin cancers, *BMC Cancer* 21 (2021) 155, <https://doi.org/10.1186/s12885-021-07866-w>.
- [36] L. Elkhadragy, H. Alsanar, M. Morel, W. Long, Activation loop phosphorylation of ERK3 is important for its kinase activity and ability to promote lung cancer cell invasiveness, *J. Biol. Chem.* 293 (2018) 16193–16205, <https://doi.org/10.1074/jbc.RA118.003699>.
- [37] S. Madsen, M.E. Nelson, V. Deshpande, S.J. Humphrey, K.C. Cooke, A. Howell, A. Diaz-Vegas, J.G. Burchfield, J. Stöckli, D.E. James, Deep proteome profiling of white adipose tissue reveals marked conservation and distinct features between different anatomical depots, *Mol. Cell. Proteomics* 22 (2023), 100508, <https://doi.org/10.1016/j.mcp.2023.100508>.
- [38] S. Moriguchi, N. Shioda, F. Han, T. Narahashi, K. Fukunaga, CaM kinase II and protein kinase C activations mediate enhancement of long-term potentiation by nefracetam in the rat hippocampal CA1 region, *J. Neurochem.* 106 (2008) 1092–1103, <https://doi.org/10.1111/j.1471-4159.2008.05440.x>.
- [39] A.S. Mendez, J. Alfaro, M.A. Morales-Soto, A.C. Dar, E. McCullagh, K. Gotthardt, H. Li, D. Acosta-Alvear, C. Sidrauski, A.V. Korennykh, S. Bernales, K.M. Shokat, P. Walter, Endoplasmic reticulum stress-independent activation of unfolded protein response kinases by a small molecule ATP-mimic, *Elife* 4 (2015), e05434, <https://doi.org/10.7554/eLife.05434>.
- [40] C. Parrado Fernandez, S. Juric, M. Backlund, M. Dahlström, N. Madjid, V. Lidell, A. Rasti, J. Sandin, G. Nordvall, P. Forsell, Neuroprotective and disease-modifying effects of the triazinetrione ACD856, a positive allosteric modulator of trk-receptors for the treatment of cognitive dysfunction in alzheimer's disease, *IJMS* 24 (2023), 11159, <https://doi.org/10.3390/ijms241311159>.
- [41] D. Crowe, Induction of p97MAPK expression regulates collagen mediated inhibition of proliferation and migration in human squamous cell carcinoma lines, *Int. J. Oncol.* (2004), <https://doi.org/10.3892/ijo.24.5.1159>.
- [42] M. Solaki, J.C. Ewald, Fueling the cycle: CDKs in carbon and energy metabolism, *Front. Cell Dev. Biol.* 6 (2018) 93, <https://doi.org/10.3389/fcell.2018.00093>.

- [43] I.C. Lopez-Mejia, S. Lagarrigue, A. Giralt, L. Martinez-Carreres, N. Zanou, P.-D. Denechaud, J. Castillo-Armengol, C. Chavey, M. Orpinell, B. Delacuisine, A. Nasrallah, C. Collodet, L. Zhang, B. Violette, D.G. Hardie, L. Fajas, CDK4 phosphorylates AMPK $\alpha$ 2 to inhibit its activity and repress fatty acid oxidation, *Mol. Cell* 68 (2017) 336–349.e6, <https://doi.org/10.1016/j.molcel.2017.09.034>.
- [44] F. Guo, D.R. Cavener, The GCN2 eIF2 $\alpha$  kinase regulates fatty-acid homeostasis in the liver during deprivation of an essential Amino acid, *Cell Metabol.* 5 (2007) 103–114, <https://doi.org/10.1016/j.cmet.2007.01.001>.
- [45] M. Nakamura, T. Liu, S. Husain, P. Zhai, J.S. Warren, C.-P. Hsu, T. Matsuda, C. J. Phiel, J.E. Cox, B. Tian, H. Li, J. Sadoshima, Glycogen synthase kinase-3 $\alpha$  promotes fatty acid uptake and lipotoxic cardiomyopathy, *Cell Metabol.* 29 (2019) 1119–1134.e12, <https://doi.org/10.1016/j.cmet.2019.01.005>.
- [46] J.C. Cable, G.D. Tan, S.P. Alexander, S.E. O'Sullivan, The effects of obesity, diabetes and metabolic syndrome on the hydrolytic enzymes of the endocannabinoid system in animal and human adipocytes, *Lipids Health Dis.* 13 (2014) 43, <https://doi.org/10.1186/1476-511X-13-43>.
- [47] S. Ghafouri-Fard, T. Khoshbakht, B.M. Hussen, P. Dong, N. Gassler, M. Taheri, A. Baniahmad, N.A. Dilmaghani, A review on the role of cyclin dependent kinases in cancers, *Cancer Cell Int.* 22 (2022) 325, <https://doi.org/10.1186/s12935-022-02747-z>.